Sidesway Web Buckling of Steel Beams

G. Y. GRONDIN and J. J. R. CHENG

ABSTRACT

The lateral stability of the tension flange of doubly symmetric beams with the compression flange braced against lateral movement was investigated experimentally and numerically. Steel beams of W360×33 (W14×22) and W360×39 (W14×26) cross-section were tested to failure. Lateral supports were provided to the compression flange to prevent lateral-torsional buckling while the tension flange was free to move laterally over its entire length. Failure took the form of sidesway web buckling. A numerical model incorporating the effect of residual stresses, initial imperfections, large displacements and material yielding was implemented using the finite element method. The model was validated by comparison with the test results. The current AISC design specification for sidesway web buckling was evaluated by comparing predicted capacities with the test results and the results of a limited parametric study performed with the numerical model. It was found that the sidesway web buckling capacity predicted using the AISC model is very conservative. Less conservative, but safe, prediction equations are proposed as possible alternatives to the current AISC equation.

Keywords: Steel beam, buckling, tension flange, inelastic, residual stresses, initial imperfections

INTRODUCTION

The first observation of instability of the tension flange of a doubly symmetric beam section loaded in bending was made in the early 1970s (Costley, 1970; Bansal, 1971). During test programs designed to investigate the lateral stability of continuous beams, unexpected failure by tension flange movement accompanied by a sudden decrease in load carrying capacity was observed. In these early tests, the failure of the beams by tension flange lateral movement was attributed to a misalignment of the loads. A closer examination of the problem later showed that the failure was not a result of second order out-of-plane effects. It could be attributed to the presence of a critical compressive stress field in the web, below the load point (Summers and Yura, 1982). Expanding on the model of local web buckling under a point load proposed by Basler, Yen, Mueller, and Thurlimann (1960), Summers and Yura (1982) proposed that the compression field in the web is analogous to a column and that the tension flange acts as a lateral spring restraint. The proposed model of a column supported at the top by a pin and at the base by a lateral spring illustrated the potential for lateral instability of a point loaded beam, braced against lateral compression flange movement. This simple model was later adopted in the AISC design specification (AISC, 1994) and is presented in some detail in the following section.

This paper presents the results of an experimental and a numerical investigation of sidesway web buckling. The experimental program and the numerical analysis were designed to assess the level of conservatism in the current AISC design standard. Modified versions of the AISC design equation are developed based on the results of the finite element analysis. These simple equations are then evaluated by a comparison with the results of a parametric study.

BACKGROUND

For a beam where the compression flange is not restrained against rotation, a simple model of a column pin supported at the top and at the bottom, and restrained laterally at the base with a spring is assumed. This model is illustrated in Figure 1. It is also assumed that the vertical load on the web is linearly distributed. This is consistent with Basler *et al.*'s (1960) assumption of a triangular vertical stress distribution in the web below a point load. Replacing this triangular load distribution by a constant load of 50 percent of the maximum load, the critical load, P_{cr}, can be expressed as:

$$P_{cr} = 2\, k_b\, h \tag{1}$$

where k_b is the lateral stiffness of the tension flange, and h is the height of the web. The lateral stiffness k_b of the tension flange can be expressed as:

$$k_b = \frac{CEI_f}{l^3} \tag{2}$$

where E is the modulus of elasticity, I_f is the moment of inertia of the tension flange about its strong axis, and l is the distance between the points of lateral support on the tension flange. The constant C reflects the type of restraint at the points of lateral support. For simple lateral supports, C takes a value of 48 and for fixed lateral supports, the value of C is 192. Assuming an intermediate value of 80, using

G. Y. Grondin, Department of Civil and Environmental Engineering, University of Alberta, Edmonton, Alberta, Canada.

J. J. R. Cheng, Department of Civil and Environmental Engineering, University of Alberta, Edmonton, Alberta, Canada.

E = 200,000 MPa (29,000 ksi), and substituting Equation (2) into (1), the following expression for P_{cr} is obtained,

$$P_{cr} = 2{,}670\, t_f h \left(\frac{b_f}{l}\right)^3 \tag{3}$$

where t_f is the tension flange thickness, b_f is the flange width and h and l are as defined above. The unit of force in Equation 3 is kilonewton (kN) and the unit of length is millimetre (mm). For the force expressed in kips and the length in inches, the constant term in Equation (3) becomes 387,000. Multiplying both sides of Equation (3) by 0.4 $(h\, t_w)^3$ and solving for P_{cr}, the equation can be rewritten in the following form:

$$P_{cr} = 6{,}670 \frac{t_w^{\,3}\, t_f}{h^2}\left[0.4\left(\frac{h/t_w}{l/b_f}\right)^3\right] \tag{4}$$

For units of force in kips and length in inches, the constant in Equation (4) becomes 967,000, which is almost identical to Equation K1-7 presented in the AISC standard with the exception of the constant term which has been taken as 960,000 in the standard. In order to account for inelastic effects, the critical load predicted by Equation (4) is reduced by 50 percent if the moment at the point of load application exceeds the yield moment capacity of the section (AISC, 1994). In addition, the magnitude of the critical load given by Equation (4) cannot exceed the load that would cause buckling of the web as a column. For the case where the flanges do not offer rotational restraint to the web, assuming that a portion of the web h wide is effective, the buckling load, P_E, of the web would be:

$$P_E = 2\frac{\pi^2 EI_w}{L_e^2} \tag{5}$$

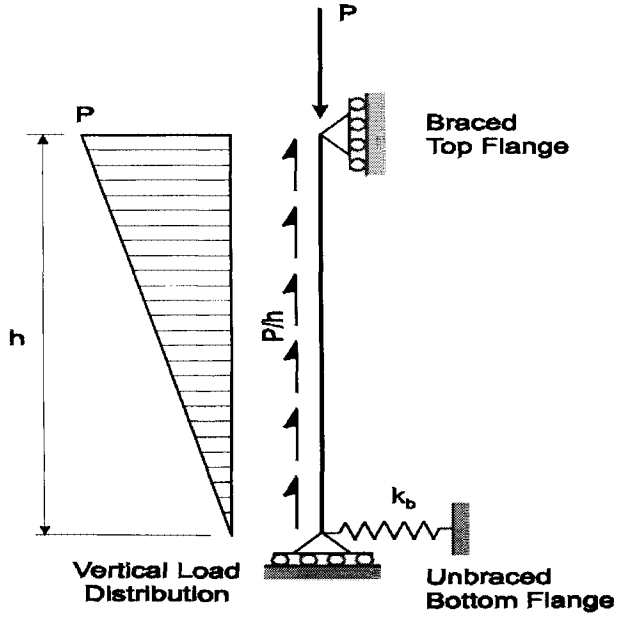

Fig. 1. Column model used by Summers and Yura (1982).

Table 1. Test Specimens Dimensions

Test	Span Length (mm)	Flange Width (mm)	Flange Thickness (mm)	Height of Web (mm)	Web Thickness (mm)
1	6,261	127	8.18	333	5.67
2	7,482	127	10.57	332	6.44
3	6,261	128	10.57	332	6.44
4	5,039	128	10.30	332	6.57

where the constant 2 is used to account for the assumed linearly varying axial load applied on the web, I_w is the moment of inertia of the effective section of the web given as $(h\, t_w^3)/12$, and L_e is the effective height of the web taken as h for the case where the bottom and top flanges do not offer any rotational restraint to the web.

The condition for sidesway web buckling can therefore be obtained from Equation (4) and Equation (5) as:

$$\left(\frac{h/t_w}{l/b_f}\right) \le 0.5\left(\frac{h}{t_f}\right)^{1/3} \tag{6}$$

If it is assumed that $h/t_f = 40$, an assumption that is generally true for economy beams, Equation (6) reverts to AISC's condition for sidesway web buckling:

$$\left(\frac{h/t_w}{l/b_f}\right) \le 1.7 \tag{7}$$

The following presents an assessment of the above model using test results obtained at the University of Alberta (Mullin and Cheng, 1994) and a finite element model validated with the test results. The finite element model was developed to expand the database of test results so that the above model could be tested for a wider range of geometric properties.

TEST PROGRAM

A full-scale test program was designed to study the lateral tension flange movement behaviour of rolled steel I-beams (Mullin and Cheng, 1994). Four full-scale steel beam specimens were tested using two different beam sizes and three different spans. The cross-sections used for the test specimens were W360×33 (W14×22) and W360×39 (W14×26). The W360×33 beam specimens were tested for span lengths of 6,260 mm and 5,040 mm, whereas the W360×39 beam specimens were tested for span lengths of 7,480 mm and 6,261 mm. The material properties were characterized using six tension coupons from each section. The average yield strength and average tensile strength of the W360×33 section were found to be 375 MPa and 538 MPa, respectively. The average yield and tensile strengths of the W360×39 were 355 MPa and 555 MPa, respectively.

Test Setup and Instrumentation

In order to create a structural system particularly susceptible to tension flange movement buckling, an end condition that provided some negative moment resistance in the plane of the beam while preventing the development of warping stresses in the ends of the bottom flange was constructed. The introduction of negative moments at the beam ends has the effect of reducing the bottom flange lateral stiffness by the introduction of compression stresses over part of the bottom flange.

A sketch of the overall test setup showing the location of the load and lateral supports is presented in Figure 2. Figure 3 shows a cross-section of the end supports. The top flange attachment was designed to resist only flexural forces. The bottom flange assembly was designed to resist both the flange flexural force and the shear force at the support. The bottom flange support assembly allowed rotation about the axis of the connection (the vertical axis), thus eliminating warping stresses in the bottom flange. The vertical shear force was carried through a thrust bearing to the reaction column while the bottom flange flexural force was transmitted to the reaction column through a tapered roller bearing. Stiffeners were placed between the top and bottom flange restraint assemblies to prevent buckling of the beam web at the supports.

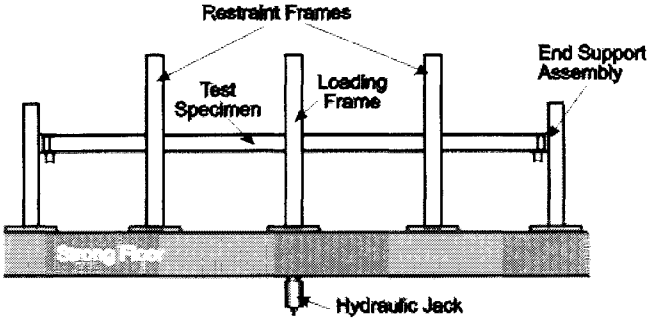

Fig. 2. Schematic of full-scale test setup.

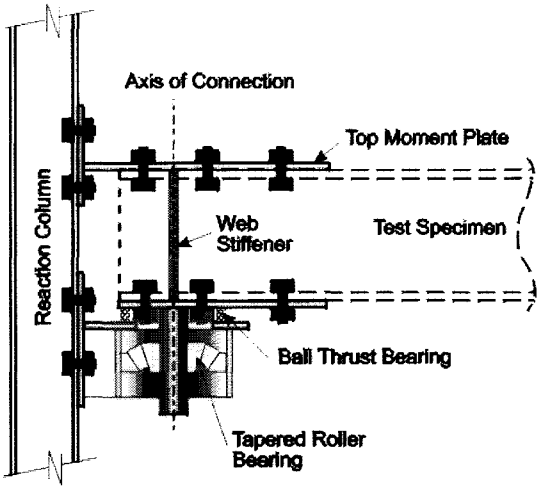

Fig. 3. Section through end support assembly.

A point load was applied at midspan through a sliding frame that provided a guided vertical movement while restraining the loaded (top) flange laterally (see Figure 4). The load was applied through rockers and rollers to allow rotation of the flange about the beam web. Displacement along the longitudinal axis of the beam was prevented at midspan. The lateral supports at quarter points allowed free displacements along the longitudinal axis and the strong axis of the member. Each brace point restrained the lateral displacement of the top flange and rotation of the beam about the vertical axis.

Instrumentation of the test specimens consisted of strain gauging five sections along the span, displacement measurement of the bottom flange along the span length, and measurement of the out-of-plane deformation of the web near the applied load. The location of the electrical resistance strain gauges and out-of-plane displacement measurements are outlined in Figure 5. Three strain gauge rosettes were placed on the web at midspan to determine the strain distribution in the web under the concentrated load. The strain measurements at

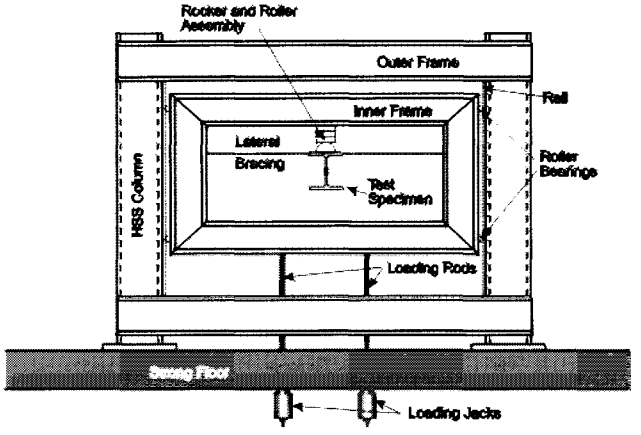

Fig. 4. Loading frame.

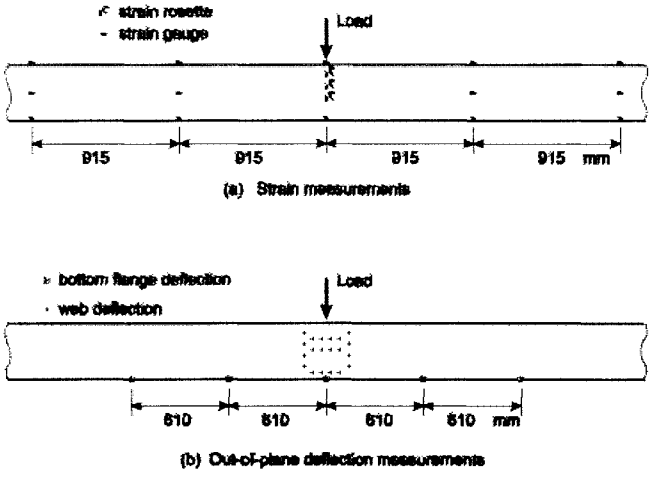

Fig. 5. Test specimen instrumentation.

Table 2. Summary of Test Results.						
Test	Section	Span (mm)	α*	Test Peak Load (kN)	Predicted Peak Load (kN) (Test/Predicted)	
					AISC	FEM
1	W360x33	6,261	0.21	112	61 (1.84)	125 (0.90)
2	W360x39	7,482	0.44	135	46 (2.93)	128 (1.05)
3	W360x39	6,261	0.08	137	80 (1.71)	143 (0.96)
4	W360x39	5,039	0.11	170	150 (1.13)	184 (0.92)
* α: Ratio of end moment to simply supported midspan moment						

the other sections along the span were used to determine the points of inflection, which, in turn, were used to evaluate the degree of fixity of the end supports. Each instrumented section, away from the section at midspan, had five strain gauges (one at mid-height and one at each flange tip). Out-of-plane deflections of the web under the load were measured at 20 locations as indicated in Figure 5(b). Bottom flange lateral deflections were measured at five locations along the beam.

FINITE ELEMENT ANALYSIS

The test specimens were modeled and analyzed using the commercial finite element code ABAQUS. The geometry of the wide flange beams was modeled with 1024 plate bending S4R elements (see Figure 6). The S4R element is a four node, doubly curved, shell element that allows for changes in the thickness as well as finite membrane strains. The model involved large displacement using a Total Lagrangian formulation. The plate material behavior was modeled by an elastic-plastic-hardening material model. Von Mises yield criterion and a kinematic strain-hardening constitutive model were implemented.

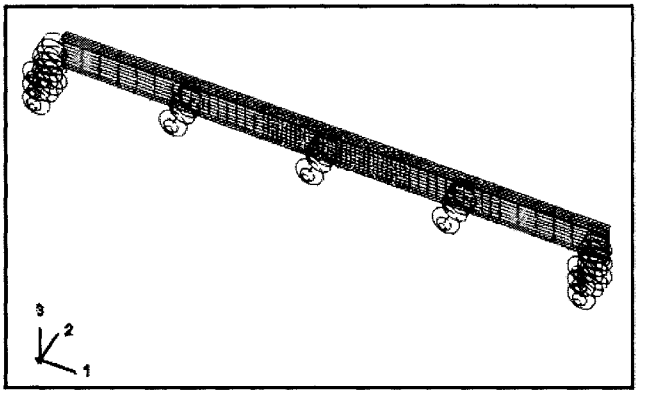

Fig. 6. Finite element model of steel beam.

In order to model the full range of behaviour of the beam, including the pre-buckling and the post-buckling regimes, the solution strategy started with a load control standard Newton-Raphson iterative procedure in the initial stage of loading, then shifted to a modified Riks procedure as the peak load was approached. The Riks procedure, also referred to as the arc length method, permits tracing the behaviour of the softening post-buckling regime.

Spring elements were used at the points of lateral restraint to simulate the flexibility of the tension rods and restraint frame assemblies were used to provide the lateral restraint in the test specimens. The end support assemblies were more difficult to model since their exact stiffness was difficult to evaluate. Referring to the end assembly shown in Figure 3, it is expected that some rotational and lateral restraints are provided by the flange connection. The lateral stiffness of the flange connection plates was evaluated based on the actual plate dimensions. They were modeled with springs placed at the top and bottom flanges in the lateral direction (direction 2 in the model shown in Figure 6). The rotational restraint contribution from the various components of the end connections was modeled with a single rotational spring placed at the centroid of the beam section at both supports. The stiffness of the rotational spring was calculated based on the location of the inflection point measured during testing. The stiffness of the end rotational spring was evaluated using the following expression:

$$k = \frac{2EI}{L}\left(\frac{\alpha}{1-\alpha}\right) \tag{8}$$

where E is the modulus of elasticity, I is the moment of inertia of the beam section about the strong axis, L is the span length of the beam, and α is the ratio of the end moment to the simple span maximum moment, which is a function of the measured

location of the point of inflection. The factor α obtained for each test specimen is presented in Table 2.

Residual Stresses

The effect of residual stresses was also included in the finite element model. The longitudinal residual stresses arising from the differential cooling of the cross-section during the manufacturing process were incorporated directly into the model. Since the residual stresses were not measured in the test specimens, the residual stress pattern shown in Figure 7 was assumed with a maximum residual stress of 30 percent of the yield strength of the material. The residual stresses were introduced in the model by imposing initial strains in the form of a temperature distribution. In order to avoid introducing transverse residual stresses in the model, an orthotropic temperature material property was used that had zero thermal expansion coefficients in directions 2 and 3, the directions perpendicular to the axis of the member. The initial strains introduce initial stresses, upon which iteration is carried out to establish equilibrium. The first load step in all of the analyses consisted of the application of the residual stresses. The following load step consisted of applying the point load at midspan to obtain the load versus deformation response of the beam both in the pre- and post-buckling regimes.

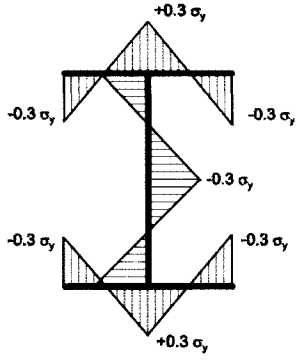

Fig. 7. Residual stress pattern used in the finite element model.

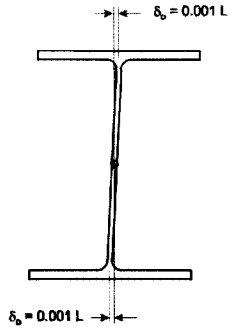

Fig. 8. Beam distortion at midspan due to initial imperfections.

Initial Imperfections

The initial imperfections in the test specimens were not measured. To account for the presence of initial imperfections in the analysis, initial imperfections in the form of lateral bending of the top flange and the bottom flange were introduced in the model. A sinusoidal wave was adopted for the shape of the initial imperfections with a maximum magnitude at midspan of 0.1 percent of the span length. The sinusoidal wave in the top flange was in the opposite direction to the one in the bottom flange. The resulting distorted shape of the beam cross-section at midspan is shown in Figure 8.

A residual stress free mesh, with the distortions described above, was first generated. The residual stresses were then applied to the beam. At the end of the first load step the deformed shape of the beam consisted of the initial imperfections described in this section plus the superimposed deformations created by the application of the residual stresses. In the second load step of the analysis the beam was loaded to failure with a point load applied at midspan.

TEST RESULTS AND COMPARISON WITH FEA RESULTS

Curves of the load versus the measured out-of-plane deflection of the tension flange at midspan are presented in Figure 9 for each of the four test specimens. The initial portion of the load versus lateral displacement plots is nearly linear. As the load approached 75 to 80 percent of the peak load, out-of-plane deflections increased at a greater rate and the out-of-plane and in-plane deflection response became distinctly non-linear. Test specimen 1 experienced a sudden lateral deflection of the tension flange of about 25 mm accompanied by a decrease of load capacity of about 10 percent of the peak load. Test specimens 2, 3, and 4 displayed stable behavior with a gradual increase in lateral deflections accompanied by a slow drop of vertical load. Since tests 2, 3, and 4 were conducted with the same beam, the tests were stopped shortly

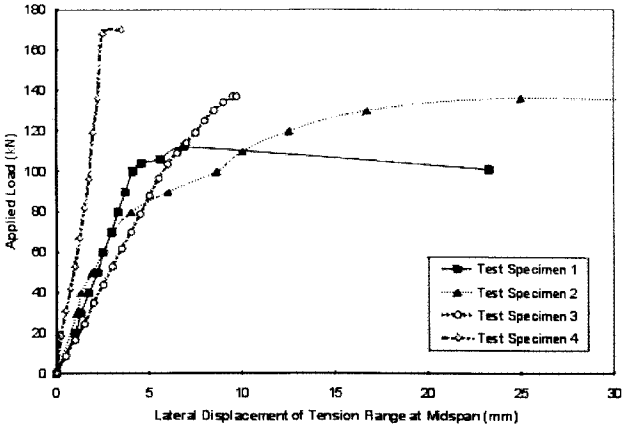

Fig. 9. Beam test results.

after a drop of vertical load was observed so that damage to the beam section would be avoided.

Strain gauges spaced at 916 mm along the length of the beams were used to determine the location of the points of inflection on the beam, from which end moments could be evaluated. The ratio of end moment to maximum simple span moment obtained for each of the test specimens is presented in Table 2. A value of 0.5 would indicate a fully rigid moment connection while a simple support would have a value of 0.0. As can be seen, the degree of fixity of the end connections varied significantly between the tests.

The finite element model described above was used to predict the test results. Figure 10 shows a comparison between the loads versus lateral displacement response obtained from the tests and the finite element analysis. A comparison of the test and predicted peak load level is presented in Table 2. With the exception of test specimen 2, Figure 10 indicates that, at the initial stage of loading, the slope of the load versus deflection curves measured for all of the specimens is lower than predicted by the finite element model. Also, with the exception of test specimen 2, the predicted load carrying capacity was higher than the measured capacity. However, the predicted capacity of the test specimens was all predicted to within 10 percent of the measured peak load. A study of the effect of initial imperfections and residual stresses, two variables that were not specifically measured in the test specimens, indicated that the difference between the measured and predicted behavior can be associated with the effect of initial imperfections and residual stresses. Considering the variability of initial imperfections and residual stresses (Tall and Alpsten, 1969) that can be expected in rolled members, the finite element model presented in the previous section is believed to be adequate to predict reliably the sidesway web buckling behavior of steel beams.

The sidesway web buckling capacity of the test specimens was also predicted using AISC's model described in Equation (4). Table 2 presents a comparison between the experimental results and the predicted capacities. AISC's model is found to underestimate significantly the tension flange buckling capacity with values of test to predicted ratios varying from 1.13 to 2.93. This is despite the fact that the test specimens were subjected to end moments that are not accounted for in AISC's equation. It is expected that the test to predicted ratios would be even greater if the beam specimens were tested without end moments. It is therefore apparent that there is room for improvement in the existing model.

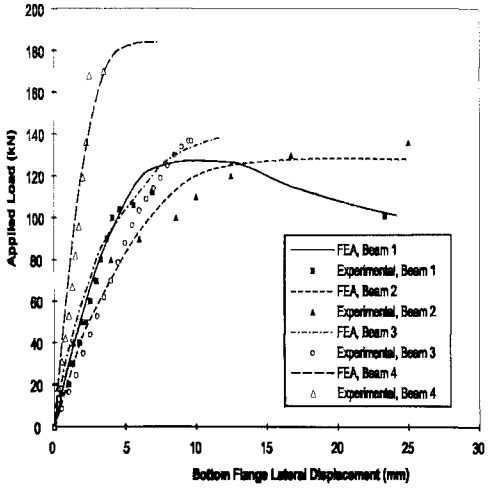

Fig. 10. Comparison of FEA predictions with the test results.

MODIFIED AISC MODEL

The finite element model was used to expand the database of test results from which modifications of the AISC model were derived. The distribution of vertical stresses in the web below the point load is shown in Figure 11. This stress distribution is typical for all four specimens from the test program. Figure 12 shows a plot of the normalized vertical stresses in the web along a section directly below the point of application of the load when the stresses were still elastic. It is evident from the figure that the linear stress assumption can be improved to obtain a better representation of the actual stress distribution in the web. In an attempt to improve upon the linear stress distribution assumed by Summers and Yura (1982), various non-linear load distributions were investigated, namely, a

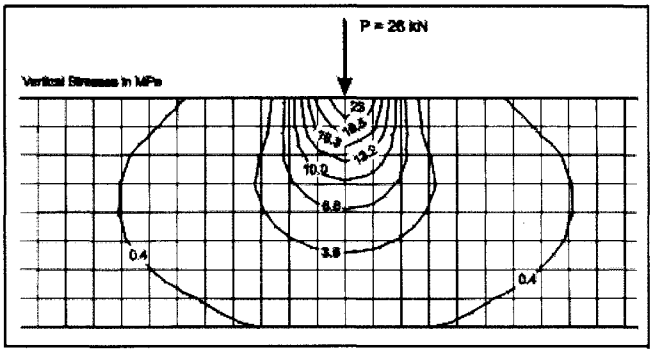

Fig. 11. Elastic vertical stress distribution under a point load.

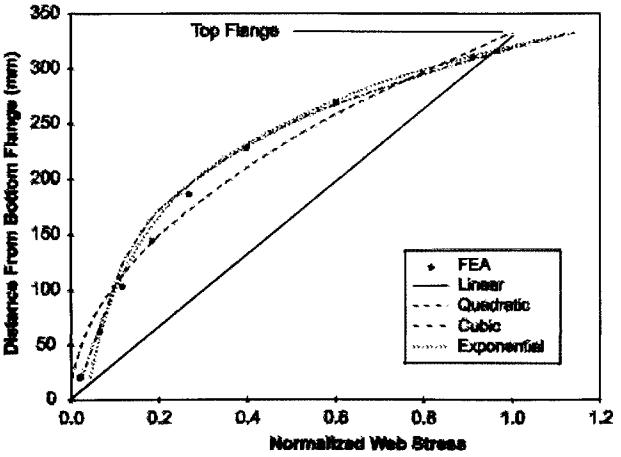

Fig. 12. Vertical force distributions in beam web under a concentrated load.

Table 3. Prediction of Test Results Using Equation (9).						
Test Specimen	α	Test Peak Load (kN)	Predicted Peak Load (kN) (Test/Predicted)			
			Linear	Quadratic	Cubic	Exponential
1	0.21	112	70 (1.6)	105 (1.1)	111 (1.0)	121 (0.93)
2	0.44	135	63 (2.1)	95 (1.4)	99 (1.4)	109 (1.2)
3	0.08	137	101 (1.4)	151 (0.91)	159 (0.86)	173 (0.79)
4	0.11	170	173 (0.98)	259 (0.66)	272 (0.62)	298 (0.57)

quadratic stress distribution, a cubic stress distribution and an exponential stress distribution (see Figure 12). Using these non-linear stress distributions and a web model similar to that proposed by Summers and Yura (1982), simple web buckling expressions can be obtained.

In addition to the change made to the vertical load distribution, modifications were also made to the web model. Rotational springs were added at the top and bottom of the rigid bar to simulate the rotational restraint provided to the web by the flanges. A translation spring was also added to the top flange to model the flexible lateral restraint provided in the test specimens. The critical load, P_{cr}, was calculated for each web load distribution discussed above using the principle of stationary potential energy. Appendix A presents a detailed derivation of the model for a quadratic web load distribution. The critical load can be expressed as:

$$P_{cr} = A\, k_b\, h \left(1 - \frac{k_b}{k_t + k_b} + \frac{k_1 + k_2}{k_b\, h^2} \right) \qquad (9)$$

where k_b is the lateral stiffness of the bottom flange and can be determined using Equation (2), k_t is the lateral stiffness provided at the top of the beam and reflects both the stiffness of the flange and the stiffness of the lateral support provided to the top flange. Since the top flange is in compression, thus reducing the lateral bending stiffness of the top flange, the stiffness k_t can be taken as the stiffness of the lateral brace. The terms k_1 and k_2 are the stiffness of rotational springs at the top and the bottom of the web, respectively. The constant A takes a value of 2.0 for an assumed linear force distribution along the web height, 3.0 for a quadratic load distribution, 3.15 for a cubic load distribution, and 3.45 for an exponential load distribution.

If one assumes that the rotational restraint offered by the flanges to the web is negligible, that the stiffness of the lateral brace on the compression flange is very large, and that the stiffness of the bottom spring, k_b, can be approximated by Equation (2), then Equation (9) reverts to Equation (4) for a linearly varying axial load on the rigid bar.

To account for the effect of yielding on the buckling capacity of the tension flange, it is assumed that the sidesway web buckling capacity is reduced by 50 percent if the moment at the point of loading exceeds the yield moment. This is consistent with the assumption made in AISC's design procedure.

ASSESSMENT OF THE PREDICTION MODELS

Equation (9) was used to predict the test results presented previously. The bottom flange lateral stiffness, k_b, was obtained from Equation (2) and the lateral stiffness at the top flange, k_t, was taken as 45 kN/mm. This is representative of the stiffness of the lateral bracing system used in the test program. The stiffness terms k_1 and k_2 were calculated assuming that the flanges are partially restrained from twisting at the end supports and free to twist along the length of the beam. The torsional stiffness of the top and bottom flanges, assuming that the ends are fully restrained, is given by:

$$k_{1,2} = 0.5128\, E \frac{b_f\, t_f^{\,3}}{L} \qquad (10)$$

where b_f and t_f are the flange width and thickness, respectively. In order to account for some flexibility in the end connections the stiffness predicted by Equation (10) was reduced by 30 percent.

Table 3 presents a comparison between the test results and the peak loads predicted using Equation (9) for a linear, quadratic, cubic, and exponential web load distribution. Except for the linear load model, all of the models overestimate the capacity of some of the test specimens. However, it should be recalled that the test specimens were partially fixed at their ends to decrease the sidesway web buckling capacity. The simple model given in Equation (9) does not account for end moments. Consequently, it is expected that Equation (9) would have the tendency to overestimate the capacity of beams that are subjected to negative end moments. As was

the case for the non-linear web load models, the linear web load model was not developed to account for beams with negative end moments. It is therefore possible that the linear web load model will overestimate the capacity of some beams with fixed end boundary conditions.

A limited parametric study, using a modification of the above finite element model, was conducted to test the ability of the above simple models to predict the sidesway web buckling capacity of beams. The modified model used for the parametric study consisted of a beam with simple end supports and perfectly rigid lateral supports at the top flange that prevented lateral displacement but allowed free rotation about the web-to-flange junction. The yield strength of the material was taken as 300 MPa. Initial imperfections, as described above, were used for this investigation. Table 4 presents the results of this parametric study where the beam length, L, the web height, h, and thickness, t_w, and the flange width, b_f, and thickness, t_f, were varied. All the cases presented in Table 4 satisfy the sidesway web buckling requirement of Equation (4). Assuming that the flanges offer negligible rotational restraint to the web (i.e. $k_1 = k_2 \cong 0$), Equation (9) can be expressed in a form similar to Equation (4) for various vertical load distributions. The critical load for the quadratic web force distribution can be obtained from:

$$P_{cr} = 10{,}000 \frac{t_w^{\,3} t_f}{h^2}\left[0.4\left(\frac{h/t_w}{L/b_f}\right)^3\right] \qquad (10)$$

The corresponding equation for a cubic distribution is:

$$P_{cr} = 10{,}500 \frac{t_w^{\,3} t_f}{h^2}\left[0.4\left(\frac{h/t_w}{L/b_f}\right)^3\right] \qquad (11)$$

and the critical load predicted for an exponential stress distribution is given as:

$$P_{cr} = 11{,}500 \frac{t_w^{\,3} t_f}{h^2}\left[0.4\left(\frac{h/t_w}{L/b_f}\right)^3\right] \qquad (12)$$

To be consistent with Equation (4) the units in Equations (10) to (12) are kN and mm. For units of force and length expressed in kips and inches, the constant term in Equations (10), (11), and (12) is 1,451,000, 1,525,000, and 1,667,000, respectively. The results of the numerical analysis and the buckling capacity predicted using Equations (4), (10), (11) and (12) are presented in Table 4. The finite element results indicate clearly that a change in web thickness leads to a significant change in buckling capacity. This, however, cannot be accounted for with the simplified models presented here since the beam web is replaced by a rigid bar in these models. The numerical analysis also indicates that the capacity of the beam increases with increasing web height, flange width, and flange thickness. An increase in span length, however, leads to a decrease in capacity. In general, the simplified models also indicate this type of behavior.

Some of the beams used in the parametric study were proportioned so that buckling of the tension flange would occur only after significant yielding of the beam. As indicated in Table 4, the predicted buckling capacity obtained from the simplified models was decreased by 50 percent to account for yielding. A comparison of the buckling capacity obtained using the simple equations with the finite element results indicates that Equation (4), the most conservative of the four equations investigated, underestimates significantly the sidesway web buckling capacity. The quadratic and cubic stress models provide intermediate predicted capacities between those predicted by the linear stress model presented in Equation (4) and the exponential stress distribution model presented in Equation (12). It can also be observed that although Equation (12) is the least conservative in most cases, it provides a safe estimate of the sidesway web buckling capacity. One exception, however, is beam R15 for which Equation (12) over-estimates the capacity. In this case, however, the capacity based on web crippling is lower than the capacity based on sidesway web buckling (325 kN for web crippling compared to 431 kN for sidesway web buckling). In this case the predicted web crippling capacity of the web is a good estimate of the capacity predicted from the finite element model. Therefore, of all the simple equations investigated here, Equation (12) gives the best prediction of the sidesway web buckling capacity of simply supported beams.

SUMMARY AND CONCLUSIONS

An experimental and analytical investigation of sidesway web buckling of steel beams was conducted. Four full-size steel beams were tested to obtain test results from which a numerical model was validated. The numerical model incorporated the effect of residual stresses, initial imperfections, inelastic material response, partial lateral restraint of the compression flange, and the rotational restraint provided at the end supports. The numerical model predicted the test results with good accuracy. The finite element model was used to determine the stress distribution in the beam web under the applied load. This information was used to develop modified versions of the Summers and Yura model to derive simple prediction models. The simple models include the effect of the top flange translational stiffness and both the top flange and the bottom flange rotational stiffness. The validated numerical model was used to perform a limited parametric study to provide a database for comparison with the prediction models, including the one adopted by AISC. Prediction models were derived for four web load distributions, namely, a linear, quadratic, cubic, and exponential distribution. The effect of web thickness was not incorporated in these simplified models. The parametric study, however, indicated that the web thickness has a significant effect on the sidesway

Table 4. Comparison of Simplified Models with FEA Results.

Beam	Beam Dimensions					Sidesway Web Buckling Capacity (kN)				
							Simplified Model			
	L (mm)	h (mm)	b_f (mm)	t_f (mm)	t_w (mm)	FEA	Eq. (4)	Eq. (10)	Eq. (11)	Eq. (12)
R1	6,000	300	100	10	5	91	37	56	58	64
R2	6,000	300	100	10	10	117	37	56	58	64
R3	6,000	300	100	20	5	162	74	111	117	128
R4	6,000	300	100	20	10	191	74	111	117	128
R5	6,000	300	150	10	5	124	62*	94*	99*	108*
R6	6,000	300	150	10	10	150	62*	94*	99*	108*
R7	6,000	300	150	20	5	228	124*	188*	197*	216*
R8	6,000	300	150	20	10	259	124*	188*	197*	216*
R9	6,000	600	100	10	5	180	74	111	117	128
R10	6,000	600	100	10	10	315	74	111	117	128
R11	6,000	600	100	20	5	283	147	222	234	255
R12	6,000	600	100	20	10	459	147	222	234	255
R13	6,000	600	150	10	5	220	124*	188*	197*	216*
R14	6,000	600	150	10	10	387	248	188*	197*	216*
R15	6,000	600	150	20	5	336	248*	375*	394*	431*
R16	6,000	600	150	20	10	594	248*	375*	394*	431*
R17	8,000	300	100	10	5	68	16	23	25	27
R18	8,000	300	100	10	10	86	16	23	25	27
R19	8,000	300	100	20	5	122	31	47	49	54
R20	8,000	300	100	20	10	142	31	47	49	54
R21	8,000	300	150	10	5	93	52	40*	42*	45*
R22	8,000	300	150	10	10	112	52	79	83	45*
R23	8,000	300	150	20	5	172	105	79*	83*	91*
R24	8,000	300	150	20	10	194	105	79*	83*	91*
R25	8,000	600	100	10	5	148	31	47	49	54
R26	8,000	600	100	10	10	219	31	47	49	54
R27	8,000	600	100	20	5	242	62	94	99	108
R28	8,000	600	100	20	10	339	62	94	99	108
R29	8,000	600	150	10	5	188	105	158	166	91*
R30	8,000	600	150	10	10	289	105	158	166	182
R31	8,000	600	150	20	5	309	209	158*	166*	182*
R32	8,000	600	150	20	10	447	209	317	333	182*

* Capacity adjusted for the effect of yielding

web buckling capacity. Of the four models investigated, the model with an exponential load distribution provides a better description of the vertical stress distribution in the web under the applied point load and leads to a better prediction of the beam capacity. The linear load distribution used in AISC leads to very conservative estimates of the beam capacity.

The present prediction equations have two shortcomings: 1) they do not account for the web flexibility and, consequently, cannot reflect the effect of the web thickness; and 2) the models are strictly applicable to simply supported beams. However, the parametric study performed using the finite element method demonstrated that, even with a web thickness as small as 5 mm, the simplified models gave conservative predictions of the buckling capacity. Therefore, although the simplified models are unable to account for changes in web thickness, they will predict the capacity of beams of various web thickness with some conservatism. Beams that develop negative end moments are more susceptible to sidesway web buckling since part of the bottom flange is in compression. Use of the equations reviewed in this report for beams with end restraint could lead to an overestimation of their sidesway web buckling capacity. This was demonstrated in a comparison with the test results. The designer should therefore use the proposed equations with caution for these cases. Further investigation of beams with end rotational restraint is required.

REFERENCES

AISC (1994), *Load and Resistance Factor Design Specification for Structural Steel Buildings*, American Institute of Steel Construction, Inc., Chicago, Il.

Bansal, J. P. (1971), *The Lateral Instability of Continuous Beams*, AISI Project 157, Department of Civil Engineering, University of Texas, Austin, Texas, 126 pp.

Basler, K.,Yen, B. T., Mueller, J. A., and Thurlimann, B. (1960), *Web Buckling Tests on Welded Plate Girders*, Bulletin No. 64, Welding Research Council, New York.

Costley, H. E. (1970), *Lateral and Local Instability of Continuous Beams*, ACE Project 157, Department of Civil Engineering, University of Texas, Austin, Texas, 74 pp.

Mullin, D, and Cheng, J. J. R. (1994), *The Effect of Tension Flange Movement on the Strength of Point Loaded Beams,* Structural Engineering Report No. 208, Department of Civil and Environmental Engineering, University of Alberta, Edmonton, Alberta.

Summers, P. A. and Yura, J. A. (1982), *The Behavior of Beams Subjected to Concentrated Loads*, Phil M. Ferguson Structural Engineering Laboratory Report No. 82-5, University of Texas, Austin, TX, August.

Tall, L. and Alpsten, G. A. (1969), *On the Scatter in Yield Strength and Residual Stress in Steel Members,* IABSE Symposium on Concepts of Safety of Structures and Methods of Design, London.

List of Symbols

A = constant used in Equation (9)
b_f = width of the tension flange
C = constant
E = modulus of elasticity
h = web height
I = moment of inertia of the beam
I_f = moment of inertia of tension flange
k = stiffness of the rotational springs at the beam ends
k_b = translational stiffness of the bottom flange
k_t = translational stiffness of the top flange
k_1 = rotational stiffness of the top flange
k_2 = rotational stiffness of the bottom flange
l = length of tension flange between points of lateral support
L = span length
L_e = effective height of the web
P_E = load that causes buckling of the web as a column
P_{cr} = sidesway web buckling load
t_f = tension flange thickness
t_w = web thickness
α = ratio of the end moment to the simple span maximum moment

Appendix A – Derivation of Buckling Load

The simplified two degrees of freedom model shown in the Figure A-1 consists of a rigid bar restrained at the top and bottom by springs of stiffness k_t and k_b, respectively. At buckling, the rigid bar adopts the configuration shown in dashed lines in the figure. The two degrees of freedom are taken as the translation at the top of the rigid element, δ_t, and its rotation, θ.

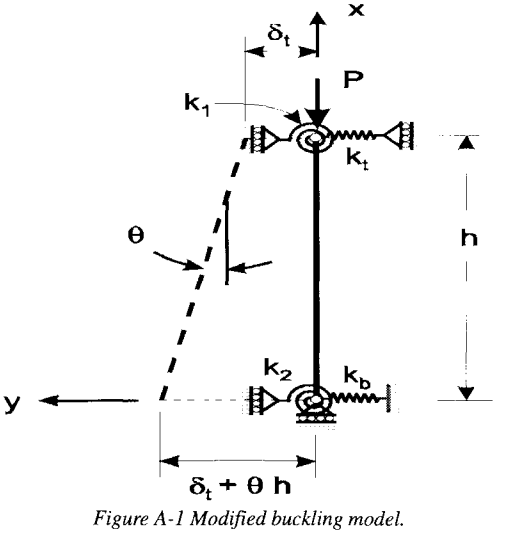

Figure A-1 Modified buckling model.

The lateral displacement of the bar at buckling, y, is given as

$$y = \delta_t + \theta\,(h - x) \tag{A-1}$$

The internal strain energy stored in the top and bottom translational and rotational springs can be expressed in terms of the degrees of freedom as follows:

$$U = \frac{1}{2}\left[(k_t + k_b)\,\delta_t^2 + (k_b\,h^2 + k_1 + k_2)\,\theta^2 + 2\,k_b\,h\,\delta_t\,\theta\right] \tag{A-2}$$

where the variables are as defined in Figure A-1. The potential energy of the external load P is given as:

$$V = -\frac{1}{2}\int_0^h P(x)\left(\frac{dy}{dx}\right)^2 dx = -\frac{1}{2}\int_0^h P\left(\frac{x\theta}{h}\right)^2 dx = -P\,\frac{h\theta^2}{6} \tag{A-3}$$

where the first derivative of y with respect to x was obtained from differentiation of Equation (A-1). Equation A-3 was obtained assuming a quadratic variation of the axial load, P, over the height, h, of the rigid bar. From Equations (A-2) and (A-3) the total potential energy is

$$\Pi = U + V = \frac{(k_t + k_b)}{2}\,\delta_t^2 + \frac{(k_b\,h^2 + k_1 + k_2)}{2}\,\theta^2 + k_b\,h\delta_t\,\theta - P\,\frac{h\theta^2}{6} \tag{A-4}$$

Using the principle of stationary potential energy, equilibrium is satisfied if:

$$\frac{\partial \Pi}{\partial \theta} = 0 \text{ and } \frac{\partial \Pi}{\partial \delta_t} = 0 \tag{A-5}$$

In matrix form Equation A-5 can be expressed as

$$\begin{bmatrix} k_b\,h^2 + k_1 + k_2 - \dfrac{Ph}{3} & k_b\,h \\ k_b\,h & k_t + k_b \end{bmatrix} \begin{Bmatrix} \theta \\ \delta_t \end{Bmatrix} = 0 \tag{A-6}$$

The buckling condition can be satisfied by setting the determinant of the coefficient matrix to zero, and solving for the axial load magnitude P. This results in the following expression for the buckling capacity of a rigid bar restrained by translational and rotational springs at the top and bottom and loaded axially with a load varying as a second order polynomial:

$$P_{cr} = 3\,k_b\,h\left(1 - \frac{k_b}{k_b + k_t} + \frac{k_1 + k_2}{k_b\,h^2}\right) \tag{A-7}$$